

Ozone Reactivity Measurement of Biogenic Volatile Organic Compound Emissions

Detlev Helmig^{1,2*}, Alex Guenther³, Jacques Hueber¹, Ryan Daly¹, Wei Wang¹, Jeong-Hoo Park¹,
Anssi Liikanen⁴, Arnaud P. Praplan⁴

¹Institute of Arctic and Alpine Research, University of Colorado, Boulder, CO 80309, USA

²now at: Boulder Atmosphere Innovation Research LLC, Boulder, CO 80305, USA

³University of California Irvine, CA, USA

⁴Atmospheric Research Composition, Finnish Meteorological Institute, 00101 Helsinki, Finland

*corresponding author: dh.bouldair@gmail.com

Revised manuscript for publication in

Atmospheric Measurement Techniques

~~March 31~~ June 20, 2022

Abstract

Previous research on atmospheric chemistry in the forest environment has shown that the total reactivity by biogenic volatile organic compound (BVOC) emission is not well considered in forest chemistry models. One possible explanation for this discrepancy is the unawareness and neglect of reactive biogenic emission that have eluded common monitoring methods. This question motivated the development of a total ozone reactivity monitor (TORM) for the direct determination of the reactivity of foliage emissions. Emissions samples drawn from a vegetation branch enclosure experiment are mixed with a known and controlled amount of ozone (resulting in e.g. 100 ppb of ozone) and directed through a temperature-controlled glass flow reactor to allow reactive biogenic emissions to react with ozone during the approximately 2-minute residence time in the reactor. The ozone reactivity is determined from the difference in the ozone mole fraction before and after the reaction vessel. An inherent challenge of the experiment is the influence of changing water vapor in the sample air on the ozone signal. A commercial UV absorption ozone monitor was modified to directly determine the ozone differential with one instrument and sample air was drawn through Nafion dryer membrane tubing. These two modifications significantly reduced interferences from water vapor and errors associated with the determination of the reacted ozone as the difference from two individual measurements, resulting in a much improved and sensitive determination of the ozone reactivity. This paper provides a detailed description of the measurement design, the instrument apparatus, and its characterization. Examples and results from field deployments demonstrate the applicability and usefulness of the TORM.

1. Introduction

Recent field research on the atmospheric chemistry in forest environments has yielded a series of results that cannot be explained with our current comprehension of biogenic emissions, deposition processes, and chemical reactions. These findings date back to the pivotal paper by Di Carlo et al. [2004] that stimulated new interest and research into the question of unaccounted for biogenic volatile organic compound (BVOC) emissions. These researchers compared the directly measured

48 hydroxyl radical (OH) reactivity in ambient air at the University of Michigan Biological Station (UMBS)
49 PROPHET forest research site with the OH reactivity calculated from a comprehensive set of
50 measured atmospheric gas phase species. The important conclusion of this study was that identified
51 compounds could only account for about 2/3 of the directly measured OH reactivity. Interestingly, the
52 difference between the two measurements, often called “missing OH reactivity” showed temperature
53 dependence very similar to that found for monoterpene (MT) compounds. This similarity led the
54 authors to hypothesize that the missing OH reactivity is due to non-identified BVOC emissions
55 emitted from tree foliage at this site.

56

57 While these findings were surprising at the time of publication, several other subsequent studies
58 have come to similar conclusions. OH reactivity measurements in ambient air have consistently
59 shown higher OH reactivity values than what can be accounted for by quantified chemical species,
60 and notably, the review of available measurements shows a tendency towards a higher discrepancy
61 at sites that are subjected to a relatively high influence from BVOC emissions [Lou et al., 2010].

62

63 The other line of research that has pointed towards the current underestimation of BVOC emissions
64 relies on ozone flux observation over forest canopies. Kurpius and Goldstein [2003] segregated
65 ozone deposition fluxes over a ponderosa pine plantation into stomatal uptake, non-stomatal surface
66 deposition, and gas phase chemistry contributions. They found that during summer, the ozone flux
67 was dominated by gas-phase chemistry, and that the ozone loss showed an exponential increase
68 with temperature, with similar behavior as BVOC emissions. However, identified BVOCs could only
69 account for a small fraction of this reactivity. Consequently, these researchers postulated that there
70 is a “large unrecognized source of reactive compounds in forested environments”. A follow-up study
71 [Goldstein et al., 2004], based on measurements during a forest thinning experiment, went even
72 further and claimed that “unmeasured BVOC emissions are approximately 10 times the measured
73 monoterpene flux”. These hypotheses have been supported by findings from a series of other
74 subsequent studies [Altimir et al., 2004; Holzinger et al., 2005; Altimir et al., 2006; Hogg et al., 2007;
75 Fares et al., 2010a; Fares et al., 2010b; Fares et al., 2010c; Wolfe et al., 2011].

76

77 There has been considerable progress in identifying and characterizing hitherto unrecognized BVOC
78 emissions. The most significant ones are light-dependent MT emissions [Ortega et al., 2007;
79 McKinney et al., 2011] and sesquiterpenes (SQT) [Duhl et al., 2008]. Furthermore, it has been
80 recognized that methyl chavicol can be strongly emitted [Bouvier-Brown et al., 2009a; Bouvier-Brown
81 et al., 2009b; Misztal et al., 2010]. However, inclusion of these emissions only contributes a minor
82 fraction to closing the gap between identified and inferred BVOC concentrations. In a study at the
83 PROPHET site, using the comparative reactivity method, Kim et al. [2011] determined directly the
84 OH reactivity in emission samples drawn from branch enclosures. OH reactivity was also calculated
85 based on BVOC emissions identified by Proton Transfer Reaction Mass Spectrometry (PTR-MS)
86 and Gas Chromatography Mass Spectrometry (GC-MS). A red oak, white pine, beech, and maple
87 tree were investigated. Their results indicated a high range of total OH reactivity from the emissions
88 of these species, with red oak emissions showing the highest OH reactivity overall. Identified
89 isoprene and MT emissions could explain the directly measured OH reactivity from red oak, white
90 pine, and beech. However, isoprene and monoterpene emissions from red maple could only explain
91 a fraction of the measured OH reactivity. The OH reactivity from maple was dominated by emission
92 of the SQT α -farnesene, which is a compound that would not have been identified in earlier studies
93 of ambient BVOC at this site. These findings show that the chemical reactivity in emissions from
94 different tree species can vary substantially in their overall magnitude and attribution to the emitted
95 BVOC species. This indicates that there is the potential that ecosystems with different plant species
96 composition could have substantial unaccounted for emissions that contribute to OH reactivity. This

97 suggests that there must be BVOC compounds or compound classes emitted from foliage that
98 current measurements do not capture, which is not unexpected given the major analytical challenges
99 associated with analysis of some organic compounds.

100

101 In this work, we are describing a monitoring approach that addresses this dilemma by constraining
102 the total ozone reactivity of BVOCs emissions with a direct measurement. These observations can
103 be contrasted with the reactivity that is calculated from the sum of the reactivities of individual BVOCs
104 and their OH reaction rates to assess the fraction of the identified and missing compounds that
105 contribute to the total reactivity. The instrument relies on a flow reactor. Sample air containing BVOCs
106 is mixed with a small flow containing a high mole fraction of ozone. The loss of ozone is monitored
107 with a differential ozone measurement. Our Total Ozone Reactivity Monitor (TORM) that was
108 previously presented in [Helmig et al., 2010; Park et al., 2013] has since undergone further testing
109 and development. The calculation of ozone reactivity is explained in Supplement A, and the modelled
110 decay of a few typically measured BVOC and ozone in the reactor is available in Supplement B.

111

112 Two other instruments relying on different types of reactor and detection methodology have been
113 reported since [Matsumoto, 2014; Sommariva et al., 2020]. These previous publications have also
114 provided the principle and reaction kinetics consideration for this measurement. A linear double-tube
115 Pyrex glass tube flow reactor with ozone detection up- and downstream of the reactor by two
116 modified commercial (ECO PHYSICS, CLD770) chemiluminescence detectors (CLD) was used in
117 the work by Matsumoto [2014]. The ozone reactivity was determined from the difference of the two
118 analyzers' signal. A 1 m long, 2.4 L volume-PTFE linear reactor, was used by Sommariva et al.
119 [2020]. These authors used two commercial Thermo Scientific Model 49i UV absorption monitors for
120 the ozone determination, with the ozone reactivity again determined from the difference of the two
121 monitor signals.

122

123 We particularly emphasize the necessity of properly characterizing the interference from water vapor
124 on the ozone determination, and the advantage of the measurement of the amount of reacted ozone
125 through a differential ozone determination with a single monitor. Thirdly, assembly of readily available
126 instrument components facilitate a relatively easy, low expense instrument assembly.

127

128 Rigid chambers or flexible bag enclosures are the common approaches for studying biogenic
129 emissions by dynamic or static vegetation enclosures [Ortega and Helmig, 2008; Ortega et al., 2008].
130 Enclosure experiments allow the selective identification of emissions from individual plant species.
131 Depending on the operational parameters, emissions can build up to many times, even order of
132 magnitudes, higher levels than in ambient air. Higher temperatures (than in ambient air) are often
133 encountered inside enclosures from the greenhouse warming effect, which enhances emissions and
134 facilitates higher sensitivity of emissions determination. An inherent disadvantage and analytical
135 challenge, however, is the evaporative water flux from the transpiring enclosed foliage. Under the
136 most extreme, and not too uncommon conditions, water vapor saturation can be achieved inside the
137 chamber, causing liquid water condensation on the chamber inside walls and within sampling tubing.
138 The water flux is sensitive to the stomatal conductance, responding to conditions of light and
139 temperature. In an ambient setting, these often change dynamically, causing similarly fast changes
140 in water vapor concentration inside the enclosure and sample air. At 30°C and water saturation, the
141 water vapor mole fraction is approximately 4.2%. A mere 10% fluctuation equates to 4.2 parts per
142 thousand (‰), or 4,200,000 ppb of a water vapor change. The signals that have been achieved in
143 ozone reactivity monitoring instruments system are usually in the single ppb range for $\Delta[\text{O}_3]$.
144 Consequently, for the ozone monitoring to be selective, the ozone detection needs to be insensitive

145 to water vapor changes that can be on the order of 10^6 - 10^7 times larger in mole fraction than the
146 ozone signal. This is an enormous challenge for this measurement, as both the ozone CLD and UV
147 absorption measurements are sensitive to water vapor.

148

149 Interference with an instrument signal response in the range of tens to hundreds of ppb has been
150 reported for different types of UV absorption monitors from rapid changes in water vapor [Wilson and
151 Birks, 2006; Spicer et al., 2010]. This interference was traced to humidity effects on the transmission
152 of light, i.e. reflectivity of light on the cell walls, through the optical cell [Wilson and Birks, 2006]. The
153 study identified that the instrument's ozone scrubber amplified this effect, acting as a water reservoir
154 adding or removing water to the air flow depending on the sample air moisture content. A 10 %
155 change in the recorded ozone was observed from a 30 to 80% RH increase for a UV absorption
156 monitor in other studies [Kim et al., 2019; Kim et al., 2020]. Inserting a Nafion dryer into the sampling
157 path can reduce the water interference, in the best scenario to within equal or better than ± 2 ppb
158 [Wilson and Birks, 2006; Spicer et al., 2010; Kim et al., 2020]. Sommariva et al. [2020] found that
159 the ozone wall losses were dependent on the relative humidity in their PTFE flow reactor.

160

161 While CLD analyzers for ozone determination are more expensive to acquire and operate, they are
162 popular for fast ozone measurements such as for aircraft [Ridley et al., 1992] and eddy covariance
163 flux measurements [Lenschow et al., 1981, 1982]. Similarly to UV monitors, CLD instruments suffer
164 from an interference by water vapor, which in this case is caused by the quenching of the
165 chemiluminescence signal in the reaction chamber [Matthews et al., 1977; Boylan et al., 2014]. A
166 correction factor of $4\text{-}5 \times 10^{-3}$ has been proposed, to be multiplied by the water vapor mole fraction
167 in nmol mol^{-1} [Boylan et al., 2014]. Under moist ambient air conditions, this correction can account
168 for up to 15% of the ozone signal. Consequently, following the enclosure system water vapor
169 estimates above, CLD in an ozone reactivity system may be susceptible to a several percent
170 interference from changing water vapor, which is on the same order of magnitude as the observed
171 ozone reactivity observed in the flow chamber system.

172

173 Both, Matsumoto [2014] and Sommariva et al. [2020] used two ozone monitors for determination of
174 the ozone upstream and downstream of the reactor, with the reacted ozone then determined as the
175 difference of the recordings from both instruments. One objective of this configuration in the
176 Matsumoto [2014] work was to achieve a reduction of the quenching interference, based on the
177 assumption that both monitors would have similar responses to the water interferences, with these
178 errors then mostly cancelling out in the differential ozone reactivity signal calculation. From a
179 measurement and signal perspective, this is a rather disadvantageous measurement approach for
180 several reasons: (1) the two monitors need to be carefully synced/calibrated against each other to
181 make sure the instrument offset is characterized and corrected for so that their readings are
182 consistent; (2) drifts of any of the two monitors, or of both, will directly transfer to a measurement
183 error in $\Delta[\text{O}_3]$; and (3), statistically, the calculation of the ozone reactivity will be subject to a relatively
184 large error, as the differential signal is a relatively small value resulting from the difference between
185 two larger numbers. Any absolute errors in the directly measured values will therefore transfer into
186 a relatively large error of the smaller differential. For these reasons, it would be preferable to measure
187 the ozone differential through a direct measurement with one monitor. Furthermore, a one monitor
188 measurement would be advantageous in terms of instrument maintenance and cost.

189

190 Our experiment presented here overcomes this predicament by modifying a commercial UV
191 absorption ozone monitor for the direct measurement of the ozone differential. Further, sample drying
192 was implemented to reduce the aforementioned interference from fluctuations in the sample water

193 vapor mole fraction. The experiments described here were conducted on two similar systems. The
194 first instrument was developed at the University of Colorado, Boulder (CU). Colleagues from the
195 Finnish Meteorological Institute (FMI) in Helsinki visited CU for collaborative research on the
196 experiment and then constructed a similar instrument to be used for their research at FMI. Both
197 groups subsequently collaborated on further characterization and improvements of the TORM, and
198 on an Arctic field deployment. In this paper, unless otherwise noted, we report experimental results
199 from the CU instrument. In cases where results from the FMI instrument are reported, those are
200 identified as FMI data. Experimental results from the CU and Helsinki instruments were compared
201 throughout the instrument development. The comparison of results and the consistency in
202 performance between the two instruments can be considered further evidence for in the
203 reproducibility of the TORM performance.

204

205 **2. Methods**

206

207 The basic principle of the ozone reactivity determination of biogenic emissions is illustrated in Fig. 1.
208 Emissions from vegetation are combined with a flow of ozone-enriched air and allowed to react in a
209 flow reactor. Ozone is measured upstream and downstream of the reactor with a single instrument.
210 In the standard configuration of an UV absorption ozone monitor, ozone-containing air and scrubbed
211 air (ozone-free air) are either measured sequentially (one optical cell) or in parallel (two cell
212 instruments), with the ozone mole fraction then determined following the Beer-Lambert Law. The
213 ozone mole fraction is proportional to the natural logarithm of the light intensity I divided from the
214 sample air (flow 1) by the light intensity in the scrubbed air I_0 (flow 2). By replacing the scrubbed air
215 flow path with a second sampling inlet line, the resulting signal no longer reflects the difference in
216 ozone between the sample (1) and scrubbed air (2, zero ozone), but instead becomes the difference
217 in ozone between the two sample flows (2-1). The required instrument modification is rather simple,
218 illustrated in Fig. 2 for a Thermo Scientific Model 49i instrument. It requires removal of the ozone
219 scrubber (MoO scrubber in most cases) and the separation of the scrubbed and sample air into two
220 separate inlets. In the standard configuration, the 49i samples air at $\approx 1.2 \text{ L min}^{-1}$ through one inlet.
221 In the modified configuration, this flow is split in half to $\approx 0.6 \text{ L min}^{-1}$ each for the Sample 1 and
222 Sample 2 inlets. An early configuration of the experiment to illustrate how the differential ozone
223 monitoring was evaluated against the monitoring of ozone up and downstream of the reactor with
224 two instruments is presented in Supplement C; the final one-monitor TORM configuration is shown
225 in Fig. 3. The direct differential ozone measurement was always conducted with a Thermo Scientific
226 Model 49i monitor. During the evaluation experiments, several different UV absorption ozone
227 monitors were used for comparing the direct measurement with a result from two individual
228 instruments. Those included Thermo Scientific Model 49i, Model 49C, and a MonitorLabs model
229 8810 monitor. The ozone that was added upstream of the reactor was generated by the Thermo
230 Scientific 49i instrument (with ozone generator option) to yield a target ozone mole fraction of 100
231 ppb. To determine the proper ozone output from the generator, an additional ozone monitor was
232 temporarily sampling the air downstream of the mixer. The ozone monitor was removed after dialling
233 the ozone output to the target level and monitoring it for several days and assuring its constant
234 output.

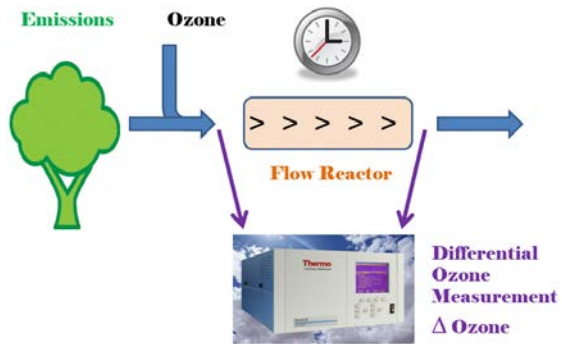
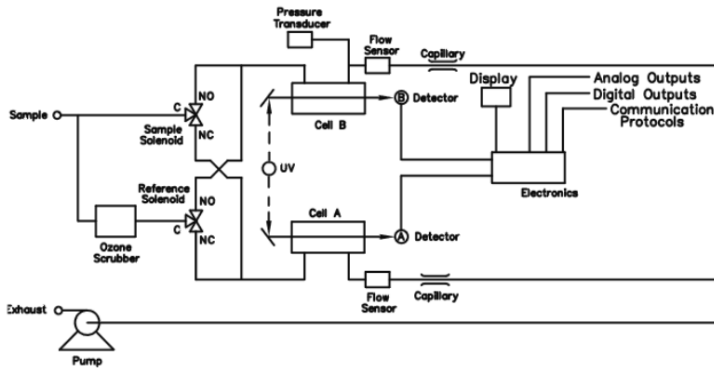


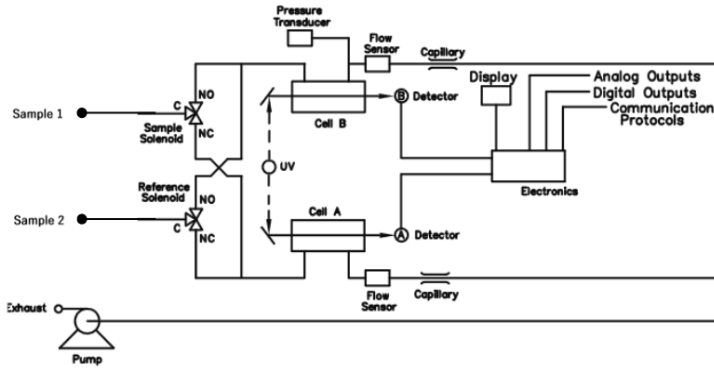
Figure 1. Principle of ozone reactivity measurement of biogenic emissions with one monitor that is configured for differential ozone signal recording.

Formatted: Font: 10 pt

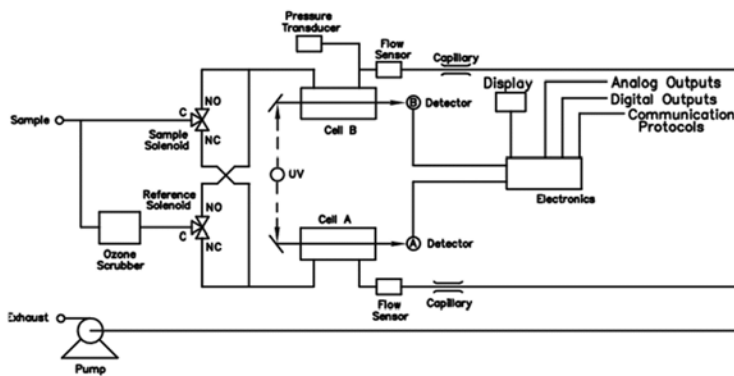
(A) Original Plumbing Configuration



(B) Differential Ozone Monitoring Plumbing Configuration



(A) Original Plumbing Configuration



(B) Differential Ozone Monitoring Plumbing Configuration

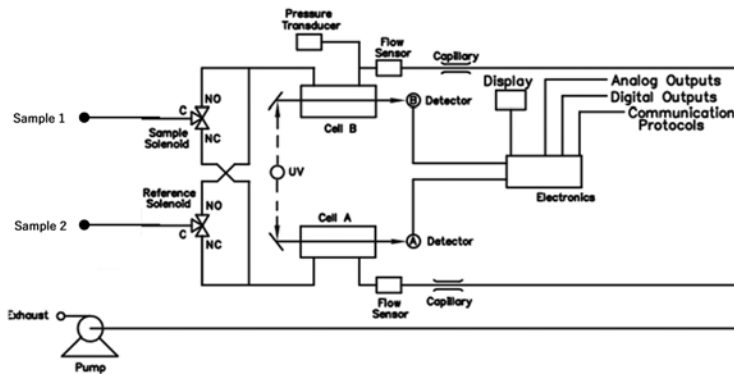
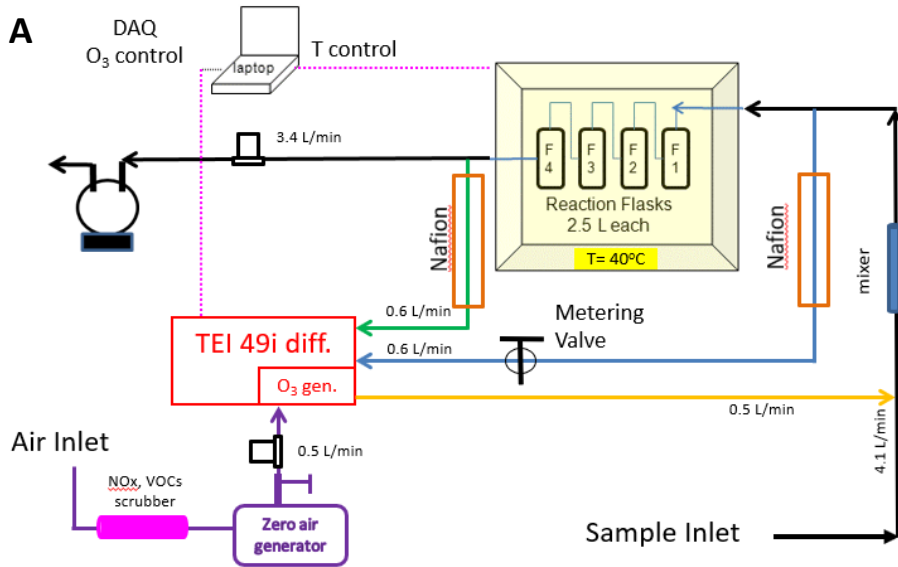
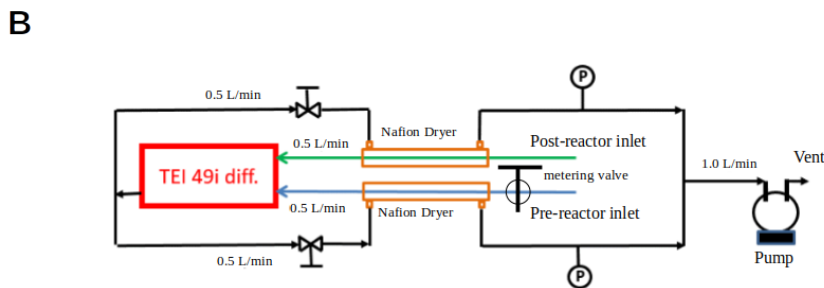


Figure 2. Plumbing configuration of a Thermo Scientific Instruments model 49 ozone UV absorption monitor in its original configuration (top) and in the modified configuration (bottom) for monitoring of ozone differentials.

235 While other studies [Matsumoto, 2014; Sommariva et al., 2020] utilized linear flow reactors, this
236 experiment relied on using four glass flasks that were plumbed in series. The glass flask reactor
237 design was chosen because it was deemed more compact and robust for field deployment
238 applications. The 2.5 L borosilicate flasks that were used are air sampling flasks that are routinely
239 deployed in the NOAA Cooperative Sampling Network for the global sampling of greenhouse gases.
240 These glass flasks have been developed and extensively tested for their inertness and purity towards
241 atmospheric trace gases (<https://www.esrl.noaa.gov/gmd/ccgg/flask.html>; flasks are fabricated by
242 Allen Scientific, Boulder, CO). Flasks are covered with shrink tubing as a protective film (polyolefin
243 shrink wrap, buyheatshrink.com) and have two ports with stopcock Teflon valves. The valve in the
244 center of the flask (Fig. 4) connects to a dip tube that leads to the inside and the opposite end of the
245 flask. This configuration allows efficient purging and replacement of the air volume inside the flasks
246 with minimal mixing. The flasks were plumbed such that the inflowing air was always introduced
247 through the dip tube. The four flasks in series add up to a total ≈ 10 L reactor volume, so that the
248 resulting residence time in the reactor is causing a sufficiently large differential signal (see also
249 section 3.5). The flasks are contained in a 45 cm x 45 cm x 45 cm (inside dimension) Pelican model
250 0340 cube case (Torrance, CA) that was fitted with 5 cm foam insulation on the inside. A rope heater,
251 temperature probe, and temperature controller allow to thermostatically control the temperature,
252 typically to 40°C. With this heating, losses of VOCs in the reactor's flasks are therefore less likely in
253 comparison to the surfaces of a branch enclosure, for example, and the tubing of the sampling line,
254 which are all at ambient temperature. The ozone reactant gas was provided from the Thermo
255 Scientific 49i monitor using its integrated ozone generator. The output was set to provide a 1000 ppb
256 constant output, so that the 1:10 dilution with the sample air flow resulted in a 100 ppb ozone mole
257 fraction entering the reactor. All experiments described in this paper were conducted at this 100 ppb
258 ozone mole fraction, unless stated otherwise. A mixer made of Teflon material (7.50 mm OD, with 30
259 mixing elements, 22.5 cm length, Stamixco AG, Wollerau, Switzerland) was inserted downstream of
260 the introduction of the ozone gas flow for providing turbulent mixing between the sample air and
261 ozone-enriched air. All tubing was made of 6.4 mm o.d./4.7 mm i.d. PFA tubing. The volume of the
262 mixer and the tubing where the sample is mixed with ozone is only of about 15 ml, so that any ozone
263 loss occurring in the tubing within a few milliseconds is negligible compared to the much longer
264 residence time (in minutes) in the much larger reactor volume. The instrument operation and signal
265 acquisition were controlled via a National Instruments digital input interface and custom-written
266 LabView software.



267



268

Figure 3. (A) Final configuration of the total ozone reactivity monitor (TORM) using one Thermo Scientific (TEI) 49i PS monitor plumbed for the direct differential ozone measurement (Figure 2), and with the Nafion dryers and metering valve included. Flow rates are indicated in the figure. Total flow through the reactor is 4 L min^{-1} . Please note that for simplicity this drawing does not show a second ozone monitor that was used for sampling the inflowing air between the mixer and the reactor to measure the ozone going into the reactor and setting the proper ozone output of the TEI 49i ozone generator. (B) Detail of the Nafion Dryer plumbing including the external pump that was added to the system for providing the purge flow for the Nafion dryers.

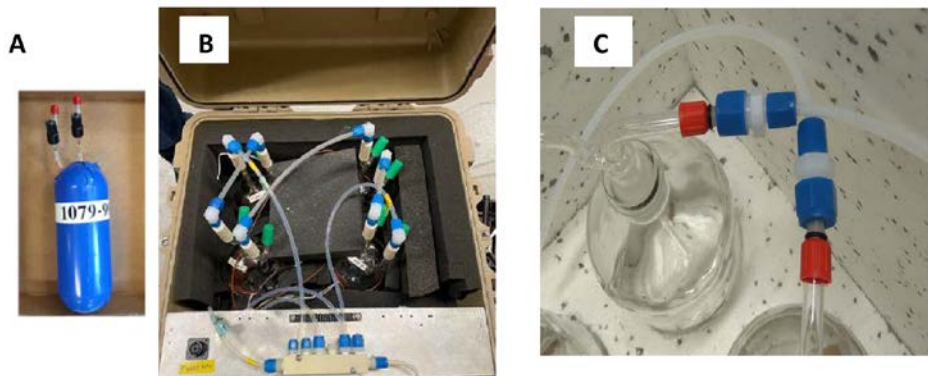


Figure 4. (A) Photograph of one of the glass flasks that were used for the University of Colorado flow reactor. (B) The ozone reactor with four of the flasks plumbed in series contained in an insulated and temperature-controlled field-deployable enclosure. Four flasks were plumbed in series for a total flow reactor volume of 10 L. (C) The 2-L bottles (borosilicate glass 3.3) used in the flow reactor system from FMI.

Experiments did not consider adding an OH scavenger (i.e. cyclohexane) [Matsumoto, 2014; Sommariva et al., 2020]. Sommariva et al. [2020] estimated a < 6 % difference in ozone reactivity for BVOC ozonolysis reactions based on modeling, but could not identify differences with and without cyclohexane added in their experiments. It is therefore unlikely that addition of an OH scavenger will make a notable difference in the ozone reactivity monitoring results.

~~A simple box model was used to estimate the expected differential signal from a known sample composition. It consists of reactions of the known BVOCs with O₃ which are solved using the kinetics pre-processor (KPP; Damian et al. [2002]). The decay of ozone after the corresponding residence time is compared to the background corrected differential signal (Supplement B).~~

During field deployments, branch enclosures were set up on sweetgum (*Liquidambar styraciflua* L.), white oak (*Quercus alba*), and loblolly pine (*Pinus taeda*) tree branches following our previously described protocol [Ortega and Helmig, 2008]. A Tedlar bag (36" x 24") was wrapped around a tree branch; the branch was situated in the middle of the bag with minimum touching of the wall. Scrubbed ambient air free of NO_x, ozone, and BVOC (Purafil and activated charcoal scrubbers), was delivered to the enclosure at 25 L min⁻¹. Most of the moisture in the purge air was also removed by condensing it in a set of coils placed inside a refrigerator. The scrubber system did not remove carbon dioxide. Air samples from the enclosure were taken through the ports affixed on the Tedlar bag, drawn at flow rates that are suitable for the sampling apparatus and instruments. The rest of the purge air escaped the enclosure mainly through the gap between the bag and the main stem of the branch.

3. Results and Discussion

3.1 System conditioning

A newly assembled system exhibited a significant ozone sink, on the order of 20-30 ppb loss of ozone (at 100 ppb) at a 4 L min⁻¹ reactor flow. The slow decline of the ozone loss signal over time indicated a gradual equilibration of the system to the ozone in the sample air. This ozone loss was

300 most likely due to reaction of ozone with impurities and active sites on interior surfaces of the tubing
301 and reactor vessel. Therefore, we chose to label it as ozone wall loss (OWL). The OWL and its signal
302 drift could almost entirely be eliminated thorough conditioning of all tubing and the reactor with an
303 air flow enriched in ozone. For this conditioning, the system was purged for 24 hours with 500 ppb
304 of ozone. After this treatment, the OWL associated with the sample flow through the reactor in the
305 absence of chemical gas reactants, i.e. the reactor background signal, was, depending on the
306 particular system condition and operational variables, on the order of 1-2 % of the supplied ozone
307 mole fraction; i.e. at 100 ppb ozone, the loss was reduced to 1-2 ppb and did no longer show any
308 drifts in the signal. The OWL recorded after system conditioning (i.e., wall losses) can be different if
309 the system is run in a different configuration (e.g., different flow through the reactor, different
310 temperature or relative humidity).

311
312 The limit of detection (LOD) for the ozone differential signal was determined from the stability of the
313 differential signal with the FMI instrument. The experiment was conducted over a full day, with the
314 reactor located outside and sampling from an empty enclosure that was purged with clean, BVOC-
315 free air and subjected to a full daily cycle of changing ambient conditions in temperature, humidity,
316 and light. There was no notable drift in the $\Delta[\text{O}_3]$ signal over the measurement period despite the
317 changes in the environmental conditions (Supplement D). After warmup, the 1-min averaged $\Delta[\text{O}_3]$
318 signal displayed a standard deviation (σ) of 0.075 - 0.096 ppb (over 1 h, $n = 60$), which corresponds
319 to a (3σ) LOD of 0.23-0.29 ppb.

320
321 Using equation (S6) from Supplement A and taking into account the dilution of sampled air with the
322 added O_3 flow, the LOD for the ozone reactivity determination can be calculated from this (3σ) signal.
323 It results in a value of $1.8 - 2.3 \times 10^{-5} \text{ s}^{-1}$. The calculation assumes an ozone mole fraction of 100
324 ppb before the reactor and a residence time of 150 s. Other systems to measure the ozone reactivity
325 using two separate monitors before and after the reactor reported slightly higher (i.e. less sensitive)
326 limits of detection, i.e. $4 \times 10^{-5} \text{ s}^{-1}$ [Matsumoto, 2014], and $4.5 - 9 \times 10^{-5} \text{ s}^{-1}$ [Sommariva et al., 2020].

327
328
329 **3.2 Balancing of the ozone monitor inlet pressures**
330

331 The readings from the differential ozone monitor are sensitive to the difference in the pressure in the
332 two sampling lines that connect to upstream and downstream of the reactor (Supplement E). The
333 pressure differential results from the vacuum generated by the sampling pump for providing flow
334 through the reactor. The 49i diagnostics menu allows monitoring of the pressures of the two optical
335 cells. In the original configuration, it was found that there was a pressure difference of, depending of
336 the flow rate, 20-30 torr between the two cells at a 4 L min⁻¹ reactor flow, with the lower pressure
337 recorded in the line downstream of the reactor. This pressure differential alters between negative
338 and positive values as the monitor alternates air from the two inlets through the two optical cells.
339 This pressure difference results in an artificial ozone signal offset between the two sampling paths.
340 An increase of the flow rate through the reactor causes a change in the pressure difference and the
341 ozone differential reported by the monitor: Increasing the flow rate from 2 to 9 L min⁻¹ corresponded
342 to an increase from 2 to 7 ppb increase in the differential ozone signal. This behavior is clearly a
343 measurement artifact and counter to the expected ozone loss, as the actual chemical ozone loss
344 decreases with decreasing residence time of the air inside the reactor (i.e. increasing flow rate). This
345 measurement artifact was mitigated by inserting a 0.64 cm Teflon metering valve into the sampling
346 line upstream of the reactor. By closing the valve slightly, the flow was restricted to where both cell
347 pressure readings from the reactor were equal (within ≈ 1 torr). This resulted in an ozone differential
348 signal of ≈ 1.7 ppb that was insensitive to the reactor flow rate (Supplement E). The final plumbing

349 configuration of the TORM and its integration into a vegetation enclosure experiment is shown in Fig.
350 5.

351 352 **3.3 Evaluation of the direct differential ozone reactivity measurement** 353

354 Results from the parallel operation of two ozone monitors measuring the actual ozone before and
355 after the reactor, with $\Delta[\text{O}_3]$ calculated from the difference of the two readings, compared to the direct
356 ozone differential measurement by TORM are summarized in Fig. 6. Field data, collected during the
357 Southern Oxidant and Aerosol Study (SOAS) (CU Boulder system), constitute a total of ten days of
358 measurements collected using branch enclosures on three different branches of sweetgum trees.
359 The OWL to the TORM was determined on five occasions by sampling from an empty bag. In these
360 field conditions, the background differential signal (3-5 ppb, Fig. 6B) was somewhat higher than in
361 the laboratory experiments described in the previous section. The OWL results bracketing the
362 vegetation enclosure experiments were averaged and subtracted from the recordings of the
363 enclosure experiments in between. The ozone differential was normalized to the air flow through the
364 chamber and to the dried weight of leaf biomass that was sampled from the vegetation in the branch
365 enclosure. These time series data show a clear diurnal cycle with the ozone differential increasing
366 steeply during daytime hours. Results are reasonably consistent between days and the three
367 different enclosures, considering that the BVOCs emissions that determine this signal are highly
368 sensitive to light and the enclosure temperature, which varied during the experiment. There is high
369 agreement between the $\Delta[\text{O}_3]$ results from both configurations across these experiments. A linear
370 regression between results from the two monitoring methods from the SOAS study yields a slope
371 value of 0.996. The graphed data also show the substantial improvement in the noise of the
372 measurement with the direct differential monitoring (A, B). The precision error of the direct differential
373 measurement is only about 1/5 compared to the result from the two monitors. After the system
374 equilibration, the 1- σ standard deviation of the differential ozone measurement for 1-min averaged
375 readings was generally in the range of 0.1 – 0.2 ppb, which was 2-3 times lower than the calculated
376 ozone difference from the two-monitor measurement. These results clearly indicate the benefits of
377 the single monitor measurement: (1) the accuracy of the differential signal is consistent with the
378 differential two-monitor determination; (2) there is a significant improvement in the measurement
379 precision from using a single monitor; and (3) the operation of a single monitor is less tedious and
380 labor intensive as it does not require the regular intercomparison for determination of offsets and
381 drifts and correction algorithms for calibrating the response of two individual monitors [Bocquet et
382 al., 2011; Sommariva et al., 2020].

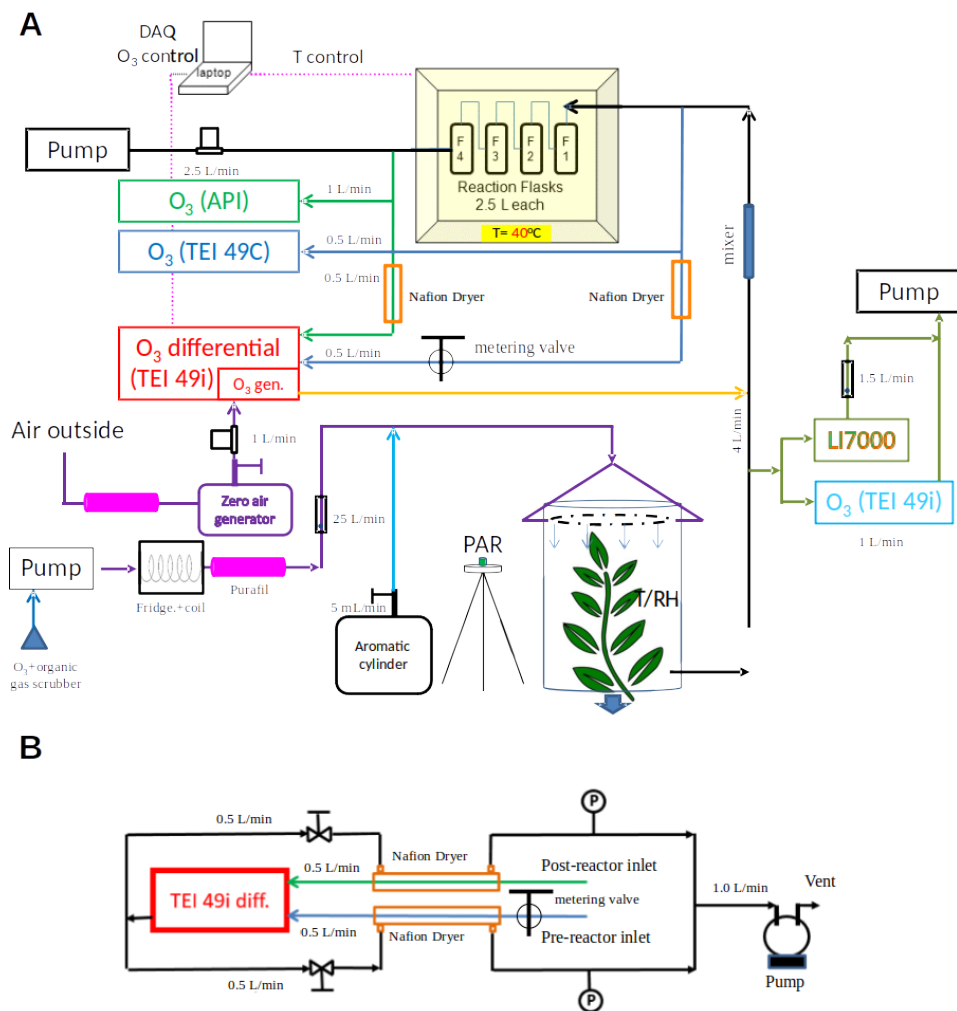


Figure 5. (A) Final configuration of the total ozone reactivity monitor with one differential ozone monitor, the sampling line pressure balancing valve, and the Nafion dryers. Note that this schematic does not include the purge flows required by the Nafion dryers. These are described separately in Figure 3B.

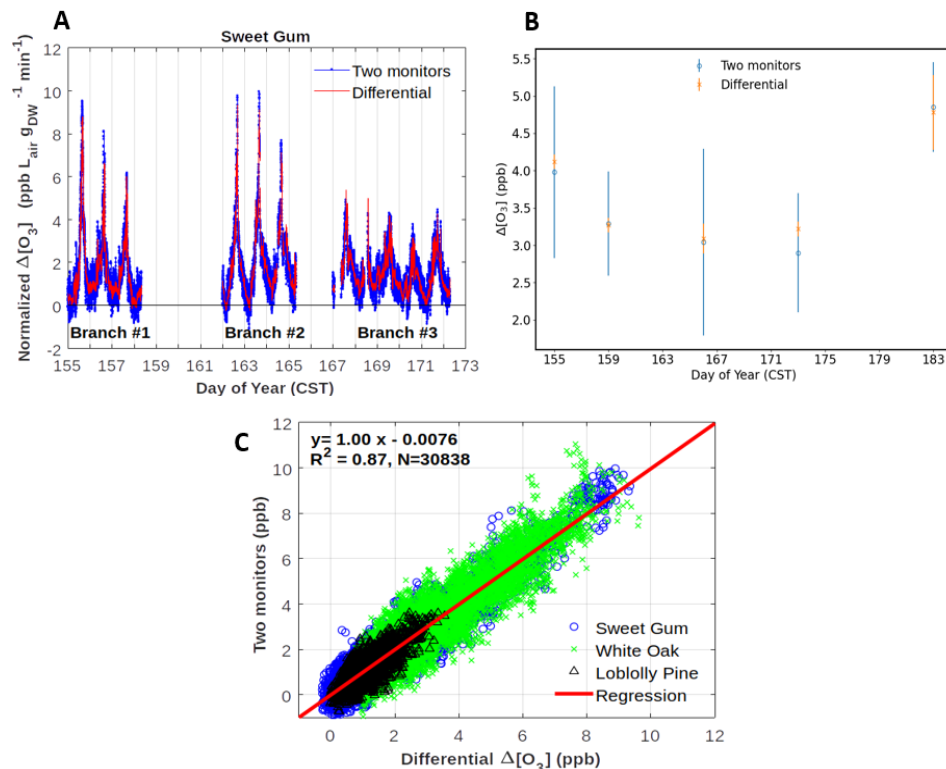


Figure 6. Results from comparisons of monitoring the ozone loss in the reactor with two monitors versus measuring the ozone differential directly with the configuration shown in Figure 2B. (A) Three multi-day experiments of $\Delta[\text{O}_3]$ monitoring from an enclosure of sweetgum branches. Data are also corrected for the empty bag OWL data shown in panel (B) and normalized for flow through the enclosure and dried weight of leaf biomass. (B) $\Delta[\text{O}_3]$ determinations from blank experiments on an empty enclosure. (C) Summary results of experiments on a total of three different vegetation species. All field experiment results are from the Southern Oxidant and Aerosol Study (SOAS) campaign between June to July 2013 at a field site in Perry County, west central Alabama (Praplan et al., in preparation).

383

384 3.4 Sample residence time in the reactor

385

386 The desired operation of a flow reactor system is for air to move through the reactor as a narrow
 387 plug, with minimal turbulence and mixing. Most flow reactors are tubular and linear and are used in
 388 laboratory settings. Depending on their operational variables, they achieve seconds to a few minutes
 389 residence time. The residence time and peak broadening during transport through the reactor was
 390 studied by installing a syringe injection port upstream of the reactor, injection of a small volume of a
 391 1 ppm standard of nitric oxide (NO), and monitoring the ozone loss from the ozone + NO reaction
 392 downstream of the reactor with a fast-response (5 Hz) nitric oxide chemiluminescence instrument.
 393 Experiments were conducted in two different configurations: 1. In the normal plumbing configuration,
 394 with the incoming air introduced to each flask through the dip tube. 2. To test the effect of the dip
 395 tube, the plumbing was also reversed. The flow through the reactor was set to 4 L min^{-1} , which for
 396 an ideal flow reactor, at 10 L volume, should result in a 2.4 min (150 s) residence time. Results of
 397 these tests are shown in Fig. 7. For both configurations, the peak signal was observed earlier than

398 the theoretical time, i.e. ≈ 18 s for the normal configuration, and ≈ 50 s for the reversed configuration.
399 The peak widths (at half of peak maximum) were ≈ 90 s and 120 s, for the normal and reversed
400 configuration, respectively. The behavior in these data show that there is a considerable amount of
401 mixing inside the reactor glass flasks, causing deviation from an ideal flow reactor. Nonetheless, the
402 residence time of ≈ 120 s for the normal plumbing configuration is sufficient to allow ozone to react
403 with the sample so that a large enough differential signal can be measured. The findings from this
404 experiment were confirmed at a higher, 6 L min^{-1} flow rate (Supplement F). Both experiments show
405 the advantage of the air introduction through the dip tube, resulting in a narrower peak, i.e. narrower
406 defined residence time.

407
408 For this configuration of the reactor, the mean residence time is about 90% of the theoretical
409 residence time. In case the flow through the reactor deviates from 4 or 6 l min^{-1} , at which these
410 experiments were conducted, a factor 0.9 is applied to the theoretical residence time in order to
411 estimate as best as possible the peak residence time for ozone reactivity calculations.
412

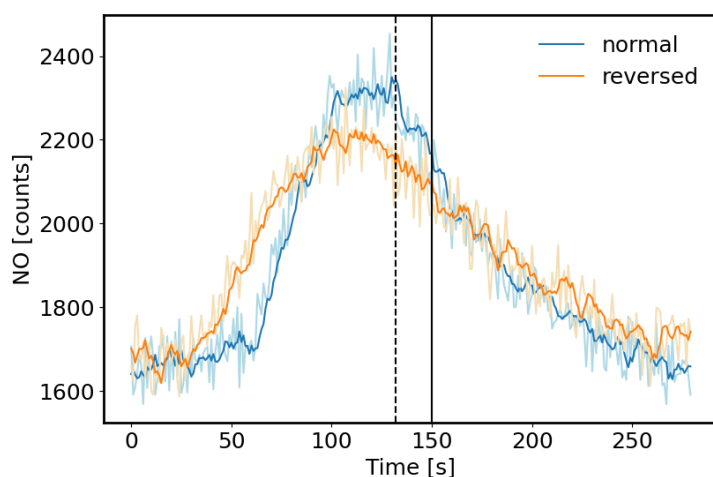


Figure 7. Test of sample air residence time in the flow reactor. A small volume of a 1 ppm NO standard was injected through a port upstream of the reactor and NO was monitored downstream with a fast response chemiluminescence analyzer (1 s time resolution). 5 s running averages are presented here. The normal configuration was with the flow entering each flask through the dip tube. The reversed configuration was with the airflow exiting each flask through the dip tube. The vertical black line indicates the theoretical residence time (150 s) based on the total flow rate (4 L min^{-1}) and total volume (10 L) of the reactor, assuming that there was no mixing inside the flasks. The dotted line depicts the mean of the distribution at 132 s for the normal configuration.

413

414 3.5 Evaluation and Mitigation of Humidity effects

415

416 As elucidated on in the introduction section, changes in humidity can severely interfere in the ozone
417 determination [Wilson and Birks, 2006; Spicer et al., 2010]. Ozone monitors have been found to be
418 less sensitive, i.e. report ozone below its actual value at high humidity, and to exhibit large artificial
419 signal fluctuations from rapid changes in the sample water vapor. Characterization and mediation of
420 the sensitivity of the ozone reactivity measurement to water vapor was a main emphasis of our
421 experiments. Earlier experiments, where the sampling flow was subjected to variable water vapor,
422 such as by injecting small volumes of water through an injection port upstream of the reactor in the

423 configuration shown in Supplement C, confirmed the findings from prior literature: Despite a constant
424 ozone mole fraction that was fed into the reactor, both, the two-monitor determination, and the single
425 monitor ozone differential determination, showed instantaneous changes in the ozone signal,
426 reaching on the order of 10 ppb. This bias in the ozone recording lasted significantly longer (≈ 10
427 times) than the residence time that was determined in the above described experiment using nitric
428 oxide, demonstrating that the retention of water, likely from reversible uptake to walls and tubing
429 inner surfaces in the reactor, is longer, and flushing water vapor out of the reactor takes a higher
430 purge volume than for less polar/more volatile gases. These water vapor effects on the ozone signal
431 were mitigated by two modifications to the TORM: (1) the glass flasks reactor was insulated and a
432 heater, regulated by a temperature controller was added to control the temperature of the reactor to
433 40°C . This heating significantly reduced the residence and interference time from the water injection,
434 likely due to a reduction of the adherence of the water vapor to the walls of the glass flasks and other
435 reactor components. Our observations agree with the findings reported by Wilson and Birks [2006],
436 who found a reduction of the water interference for their 2B Technologies ozone monitor when the
437 glass optical cell was slightly heated; and (2) Nafion dryers (0.64 cm o.d. x 180 cm length; MD-110-
438 72739 gas dryer, Perma Pure LLC, New Jersey, USA) were inserted into both ozone monitor inlet
439 flows before and after the reactor. We installed the two Nafion dryers there, rather than one Nafion
440 dryer for the sample flow path going into the reactor, to prevent possible losses of polar and
441 unsaturated compounds from the sample flow passing through a Nafion dryer, as has been reported
442 in other prior research. The purge flow for the Nafion dryers was provided by the vent flow from the
443 TEI 49i. The analyzer vent flow was split into two approximately equal fractions, resulting in 0.6 L
444 min^{-1} flow for each Nafion Dryer (Figure 5B). Throttle valves were installed in both lines as flow
445 restrictors and adjusted such that the pressure in the exterior chamber of the Nafion dryers was
446 $\approx 10\%$ below the interior section of the dryer (cell pressure readings from the differential 49i monitor).
447 The Nafion dryers were conditioned using the same protocol as for the reactor (see above), after
448 which there was no notable ozone loss from sampling the ozone-enriched air flow through the Nafion
449 tubing, in agreement with other previous studies that have reported negligible ozone loss in Nafion
450 tubing materials [Wilson and Birks, 2006; Boylan et al., 2014; Kim et al., 2020].

451
452 Results from an experiment with the Nafion dryers in use and where water vapor was increased in
453 multiple steps is shown in Fig. 8. The same humidification system as described by Boylan et al.
454 [2014] was used for moisturizing a zero air dilution gas fed to the TORM. The resulting humidity was
455 recorded with a LICOR model 7000 $\text{CO}_2/\text{H}_2\text{O}$ gas analyzer downstream of the mixer, but upstream
456 of the reactor. Each humidity level was maintained for 30 min, before subjecting the system to the
457 next higher moisture level by a rapid change in the humidity generator setpoint. The differential signal
458 was monitored with the differential 49i monitor, as well as by recording the absolute ozone upstream
459 and downstream of the reactor with two individual monitors. Both ozone monitoring systems were
460 sampling through the Nafion tubing. Results of the experiment (Fig. 8) show a residual differential
461 signal response of ≈ 0.5 ppb over an approximately 10 to 84 % RH span for the differential monitor.
462 The two-monitor $\Delta[\text{O}_3]$ response is approximately six times as large. The spikes seen during the
463 moisture transition periods seen in earlier experiments disappeared completely for the differential
464 monitor. If background measurements are performed at a different RH than the ozone reactivity
465 measurements, this residual differential signal needs to be taken into account on a case-by-case
466 basis.

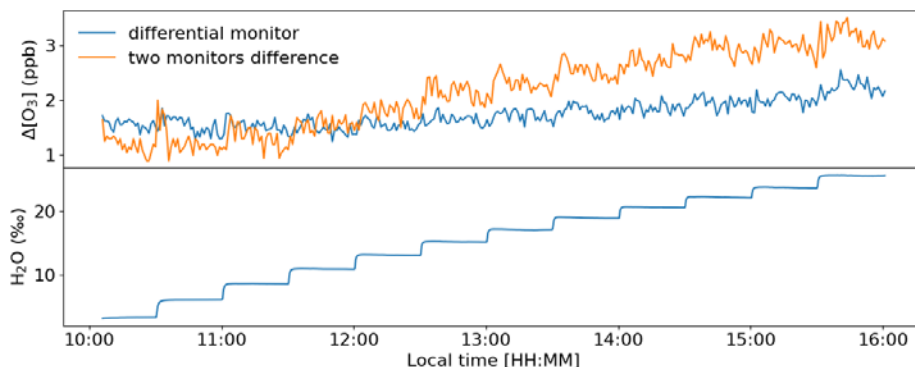


Figure 8. Experiment with increasing humidity in the air supplied to the TORM. The humidity content of the sample air is displayed in the lower graph in units of parts per thousand (‰). A total of 12 levels were administered, from ≈ 3 -26‰, which at room temperature conditions (25°C) is approximately equivalent to a RH range of 10-84%.

467

468 Similar order of magnitude results were obtained in a series of experiments where liquid water (20
 469 to 100 μl) was injected into the sampling flow through a septum port upstream of the reactor. The
 470 Nafion dryer removed $\approx 2/3$ of the water interference, and the differential monitor response to the
 471 water injection was less than half compared to calculated difference from the two-monitors
 472 configuration (Supplement G).

473

474 3.6 Application Examples

475

476 Ozone reactivity of test mixtures and samples from vegetation enclosures were investigated in
 477 laboratory and field systems. A laboratory experiment using a flow of limonene standard test gas is
 478 presented in Fig. 9. The purpose of the experiment was to demonstrate the linearity of the TORM
 479 response and to derive a lower bound estimate for the TORM response. Here, we chose to define
 480 the TORM response (in units of ppb s) as the delta ozone signal (ppb) per unit of ozone reactivity (s^{-1}),
 481 as calculated from the product of the reactant mole fraction and its ozone rate constant. The test
 482 gas standard was prepared in house for a target mole fraction of 20 ppm. However, but the actual
 483 mole fraction is expected to have decreased with time, but could not be independently verified at the
 484 time of the experiment. The theoretical mole fractions, after mixing of the standard with the dilution
 485 flow, range between 0-33 ppb, which is a typical range observed during enclosure experiments) and
 486 represents upper limit values. The TORM determination shows good linearity, with a R^2 result of the
 487 linear regression of 0.99941.00. At the highest limonene level, the TORM signal, recorded with the
 488 differential ozone monitor, was 0.91.1 ppb (after subtraction of the 1.7 ppb Δ ozone reactor
 489 background OWL that was determined for this particular application), which corresponds to a total
 490 O_3 reactivity of $7.3 \text{ e}^{-5} \text{ s}^{-1}$, considering $[\text{O}_3]_0$ to be 100 ppb and the residence time 150 s (3.6 l min^{-1}
 491 flow through the 10 L reactor, scaled with a factor 0.9). This infers that the limonene mixing ratio
 492 entering the reactor would be 13.6 ppb, which is reasonable considering the dilution from the gas
 493 standard (8.4 ml min^{-1} standard flow in a 5.1 l min^{-1} total flow) and its target mole fraction.

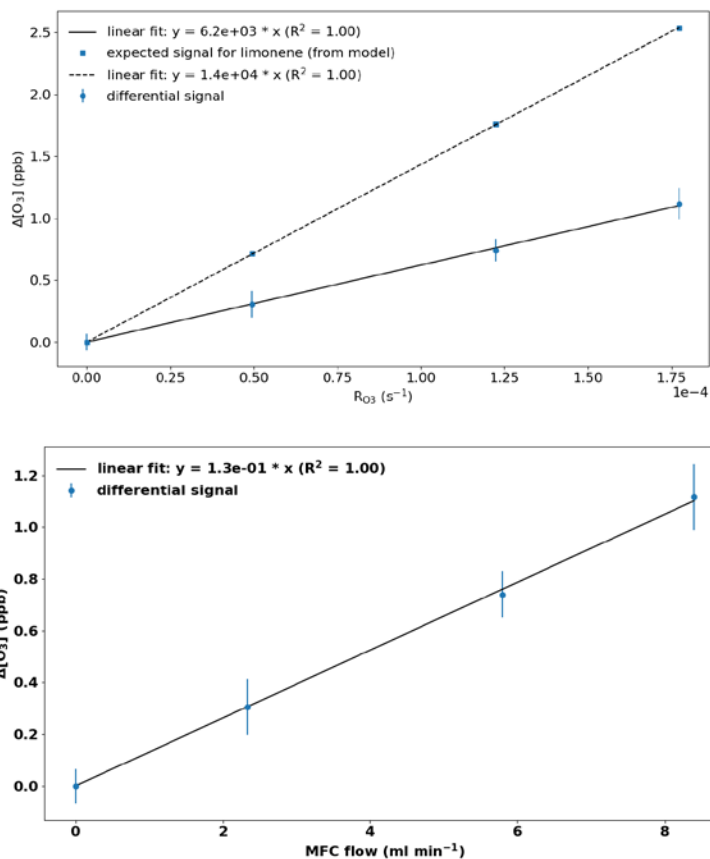


Figure 9. Laboratory test of the TOM. A small flow of a high mole fraction limonene standard was fed into the system upstream of the reactor. The theoretical reactivity calculated from the BVOC ozone rate constant, ozone mole fraction, and residence time are given on the x-axis. Error bars represent the standard deviation for the monitoring data at each level.

In Fig. 9, the experimental results from the limonene experiments are also compared with the modelled signal for various O_3 reactivity values for limonene for the operating conditions of TOM during this experiment. The modelled results reflect the expected O_3 decrease due to the reaction with limonene after the reaction corresponding to the residence time in the reactor (here 150 s; $3.6\ l\ min^{-1}$ flow through a 10 L reactor, scaled with a factor 0.9). The applied rate constant for the reaction of ozone with limonene at 298 K is $21 \times 10^{17}\ cm^3\ s^{-1}$ [Atkinson and Arey, 2003]. A linear regression shows that $\Delta[O_3]$ is linearly dependent with R_{O_3} (slope value of $1.4 \times 10^4\ ppb\ s$). The discrepancy between the model and the experiment stem likely from the uncertainty of the mixing ratio in the limonene standard. The experimentally determined response of the differential monitor, i.e. $6.2 \times 10^3\ ppb\ s$, is therefore a lower limit. Applying a lower limonene mole fraction in the standard would lead to a proportionally higher value.

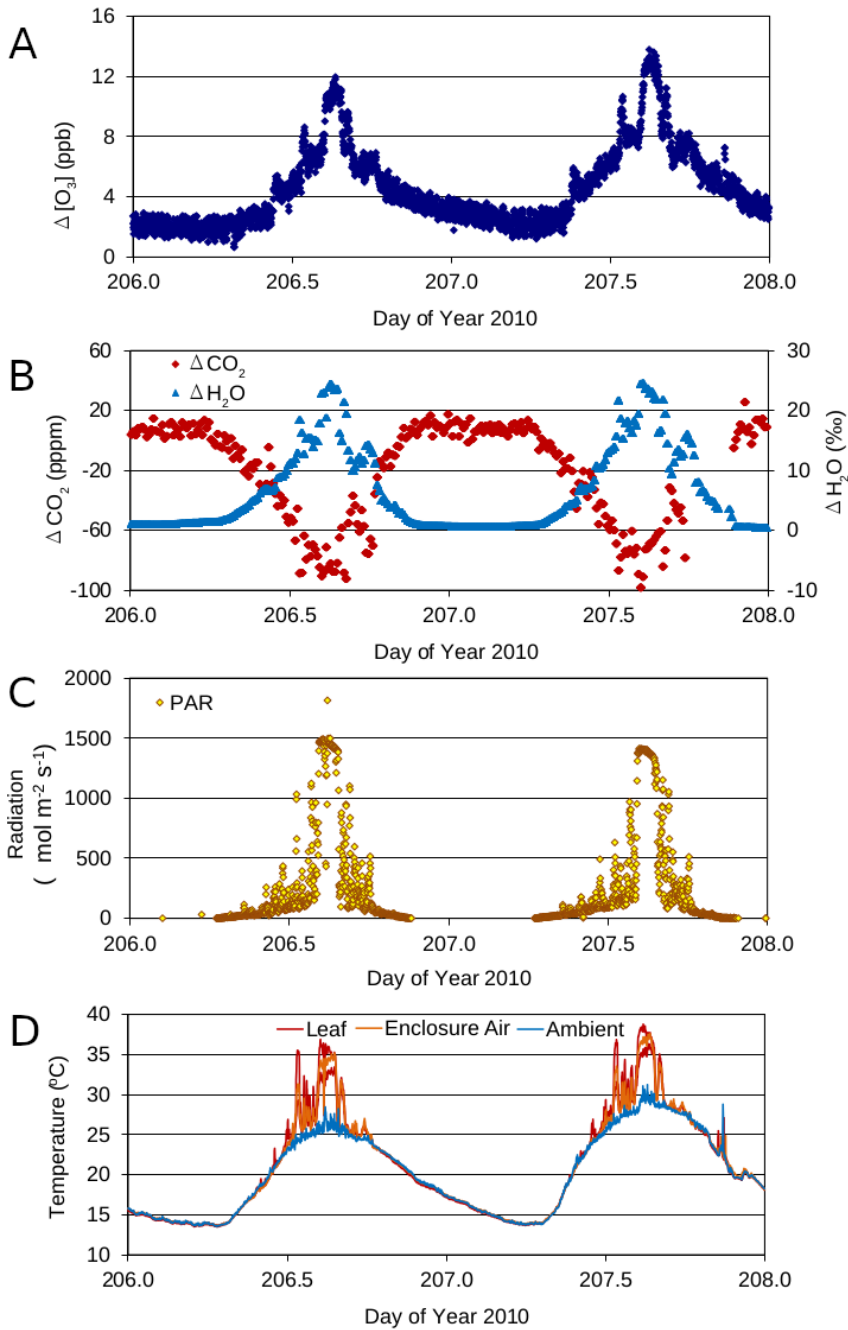
Formatted: Figure

Formatted: Font: 10 pt, Not Italic

494
495
496
497

The TOM has been deployed in field settings at several research sites in the U.S. and in Finland. Figure 10 displays more results from one of these field experiments, i.e. a 3-day branch enclosure experiment on a red oak tree at the University of Michigan Biological Station. These data show

498 ~~results from the 2nd and 3rd days of the experiment. (UMBS) in 2010.~~ The experiment was conducted
499 on relatively warm and sunny days as can be seen in the radiation and temperature data. Besides
500 the differential signal, ~~and the calculated total ozone reactivity, both~~ shown in panel A, ~~the figure also~~
501 ~~includes (differential signal scale on the left, and total ozone reactivity scale on the right),~~ the
502 concurrent measurements of respiration and photosynthesis ~~(B),~~ photochemical active radiation
503 (PAR) ~~(C),~~ as well as ambient, leaf and enclosure ~~temperatures (D).~~ ~~temperature.~~ The change in
504 humidity, reaching a maximum of on the order of 25‰ as the mid-day maximum when foliage
505 respiration peaks, confirms our estimate presented in the introduction section for the humidity
506 changes during vegetation enclosure experiments. Emission samples collected from this enclosure
507 and analyzed by gas-chromatography showed that emissions from this branch were dominated by
508 isoprene, with further substantial emissions of MT and SQT compounds. On both days, the TORM
509 recorded a mid-day maximum differential ozone signal of 12-14 ppb, dropping to 2-3 ppb at night.
510 ~~The instrument readings are quite similar on both days, which is close to the system background~~
511 ~~signal (OWL).~~ The differential signal clearly follows a daily cycle, with low values during nighttime
512 hours, and daytime maxima during the early afternoon. The ozone reactivity signal maxima coincide
513 with the peak in diurnal radiation, respiration, and photosynthesis, which suggests that the ozone-
514 reactive emissions are modulated by light availability. ~~Comparison of the observed ozone reactivity~~
515 ~~with the calculated~~

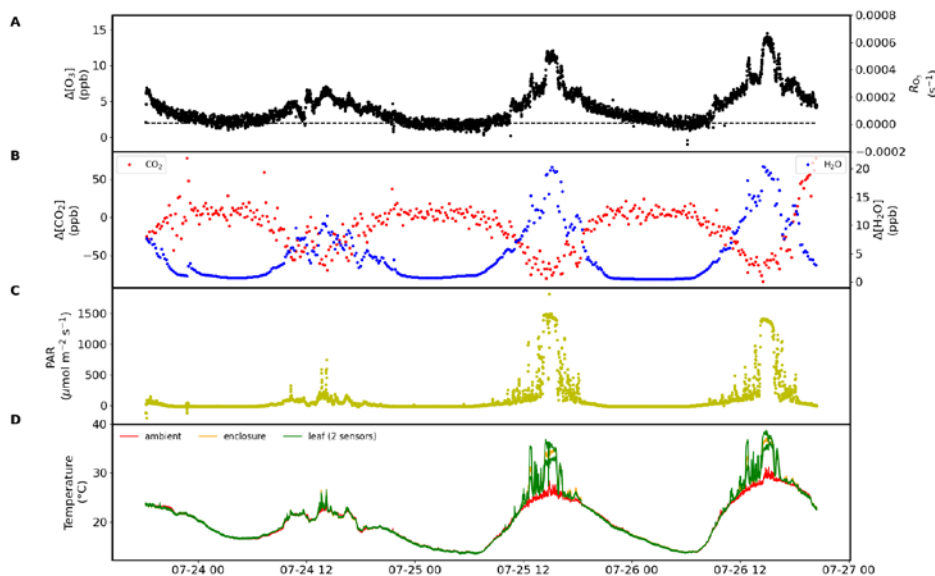


516 **Figure 10.** Results obtained over two days from a branch-enclosure experiment on a red oak tree, with data
 517 for $\Delta[\text{O}_3]$ measurements (A), solar radiation (B), respiration and photosynthesis expressed as the difference in
 518 the water and CO_2 mole fractions in the air stream going into and out of the enclosure (C), and leaf, inside
 519 enclosure, and ambient temperature (D).

520 ozone reactivity from identified BVOC species could only account for a fraction of the observed
521 reactivity (Praplan et al., manuscript in preparation). Similar diurnal cycles of ozone reactivity were
522 observed for sweetgum in the Southern Oxidant and Aerosol Study [Park et al., 2013], as can be
523 seen in the ten days of measurements shown in Fig. 56. Please note that the data in Fig. 56 were
524 normalized to the leaf dry mass of the enclosure foliage. A detailed discussion comparing the
525 observed total ozone reactivity with the ozone reactivity calculated from identified BVOC species in
526 the emissions is the subject of an upcoming publication (Praplan et al., manuscript in preparation).

527 A presentation of the ozone reactivity results normalized to the leaf dry mass and
528

Formatted: Font: 10 pt, Bold



529 **Figure 10.** Results obtained over three days from a branch enclosure experiment on a red oak tree at the
530 University of Michigan Biological Station, with (A) results for the $\Delta[O_3]$ measurement, with the dashed black
531 line indicating the value of the wall losses/background (left) and the corresponding R_{O_3} (right), (B) respiration
532 and photosynthesis expressed as the difference in the water (right) and CO_2 (left) mole fractions in the air
533 stream going into and out of the enclosure, (C) solar photosynthetically active radiation (PAR), and (D) leaf,
534 inside enclosure, and ambient temperature.
535
536

537 Furthermore, a presentation of the ozone reactivity results normalized to the leaf dry mass and flow
538 through the branch chamber as a function of leaf temperature for experiments performed at UMBS
539 is shown in Fig. 11. All four species show an increase of reactivity with increasing temperature. This
540 feature indicates that all species emit reactive volatiles at increasing rates as temperature increases.
541 Interestingly, the normalized reactivity for the various tree species is quite different, varying by at
542 least a factor of three. It also appears that the temperature dependencies are different, with red
543 maple showing a more dynamic increase than other species. Remarkably, white pine, a high MT
544 emitter, gave the lowest reactivity results. Furthermore, red the ozone reactivity temperature
545 response for red maple results appear appears to be higher than for red oak, despite the fact that red
546 oak was found to emit high higher amounts of BVOC, totalling $\approx 100 \times$ those of than maple, but with
547 most of the emissions made up by isoprene. The relatively high levels of ozone reactivity are also
548 noteworthy in light of the independent OH reactivity study by Kim et al. [2011], who found that red
549 maple emissions exhibited the highest missing OH reactivity associated with SQT in comparison
550

551 with these other three species. Consequently, red maple is a prime candidate for having reactive
552 BVOC emissions that hitherto have not been chemically identified.

553
554

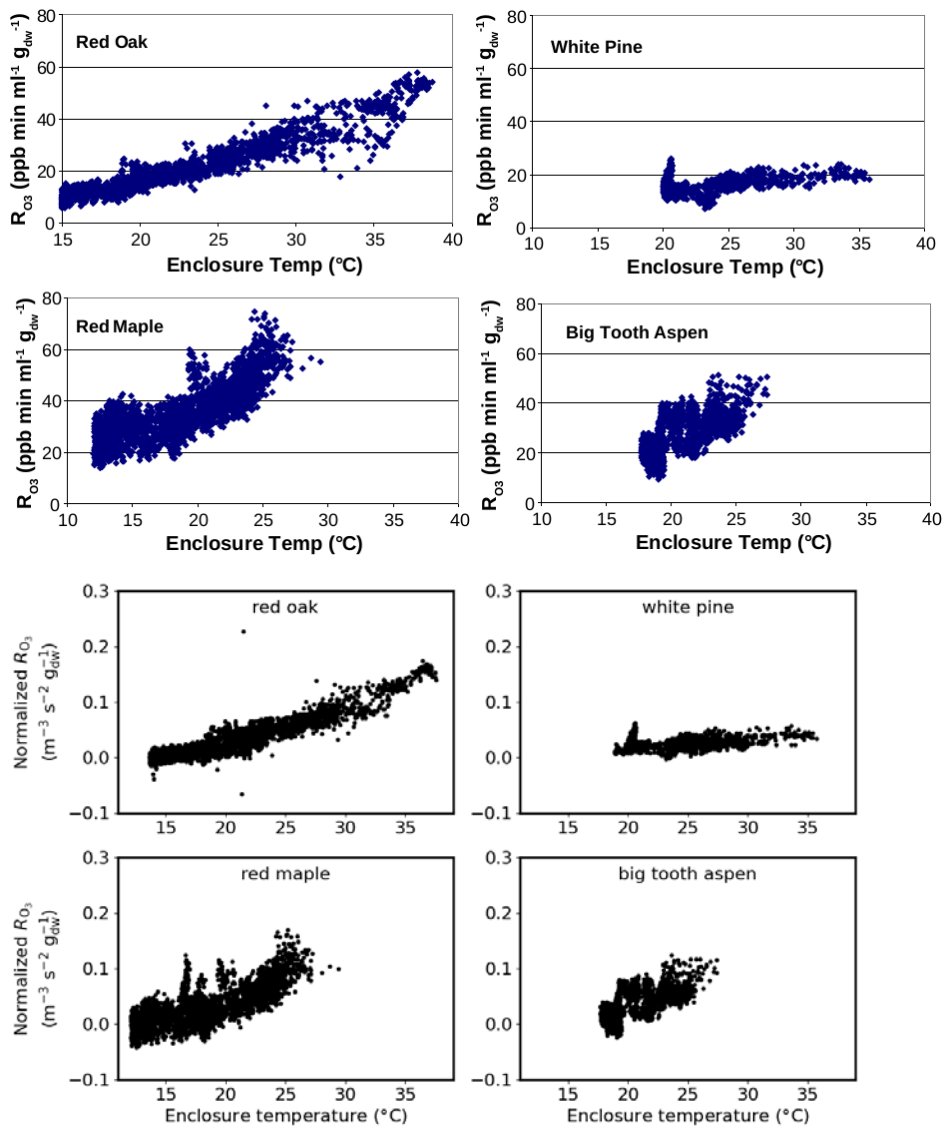


Figure 11. Delta-ozone Total O₃ reactivity from the emissions results from experiments on red oak, red maple, white pine, and big tooth aspen at the University of Michigan Biological Station, normalized to the amount of leaf dry mass and flow rate, as a function of enclosure temperature.

555

556 **4. Summary and Conclusions**

557
558 A total ozone reactivity monitor, TORM, was developed for the study of the ozone reactivity of
559 biogenic emissions. TORM builds on standard laboratory equipment and can be assembled with
560 moderate technically skilled personnel and at relatively moderate cost. The instrument was
561 thoroughly characterized, and a number of ameliorations were implemented that significantly
562 improved the measurement sensitivity and reduced the interference from absolute and changing
563 water vapor in the sample air. Critical improvements over previously reported measurement
564 approaches were the adaptation of a commercial ozone UV absorption monitor for direct
565 measurement of the reacted ozone (ozone differential), heating and temperature control of the
566 reactor, and the drying of the sample flows with Nafion dryers. Specific challenges arose with this
567 setup that could be overcome, such as balancing the pressure difference for each cell in the
568 differential ozone monitor (one cell measuring before the reactor and the other cell measuring after).

569
570 TORM has been used in a number of field settings and proven the feasibility and value of this new
571 measurement. Differential ozone signals ($\Delta[\text{O}_3]$) on the order of 0-5 ppb have been obtained in
572 enclosure experiments on high-BVOC emitting species. These signals are 20-50 times above the
573 noise level of the measurement. Chemical identification of BVOC emissions from the enclosure and
574 estimation of the total reactivity of identified emissions has been able to only account for a fraction
575 of the directly measured ozone reactivity. Detailed description of these field studies and discussion
576 of the results, including the attribution of the directly measured ozone reactivity to identified BVOC
577 emissions, will be presented in a forthcoming publication (Praplan et al., in preparation).

578
579

580 **Data availability**

581
582 All data that the work builds on are presented in the manuscript and Supplemental Information.

583

584 **Disclaimer**

585
586 This study does not necessarily reflect the views of the funding agencies, and no official
587 endorsements should be inferred.

588

589 **Funding Information**

590
591 The development and testing of the TORM system has been made possible through funding from
592 the U.S. National Science Foundation, grants #AGS 0904139, ATM-1140571, and AGS-1561755,
593 as well as funding from the Academy of Finland (decisions nos. 307797 and 314099).

594

595 **Author contribution**

596

597 D.H. Principal Investigator of the U.S. study, advised student researchers, managed research grants,
598 oversaw the study, prepared and approved the manuscript.

599

600 A.G. Co-Principal Investigator of the U.S. study, reviewed and approved the manuscript.

601

602 J.H. Constructed instrumentation and conducted experiments, developed control and data
603 acquisition software, approved the manuscript.

604

605 R.D. Constructed instrumentation and conducted experiments, participated in field studies, reviewed
606 and approved the manuscript.

607
608 W.W. Constructed instrumentation, conducted experiments, prepared, reviewed, and approved the
609 manuscript.
610
611 J.H.P. Constructed instrumentation, developed instrument control software, conducted lab and field
612 experiments, reviewed and approved the manuscript.
613
614 A.L. Constructed instrumentation, conducted lab and field experiments, approved the manuscript.
615
616 A.P.P. Principal Investigator of the Finnish study, conducted field and lab experiments, prepared and
617 approved the manuscript.
618
619 **Competing Interests**
620
621 The authors declare that they have no conflict of interest.
622
623 **References**
624
625 Altimir, N., P. Kolari, J. P. Tuovinen, T. Vesala, J. Back, T. Suni, M. Kulmala, and P. Hari (2006), Foliage surface
626 ozone deposition: a role for surface moisture?, *Biogeosciences*, 3, 209-228.
627 Altimir, N., J. P. Tuovinen, T. Vesala, M. Kulmala, and P. Hari (2004), Measurements of ozone removal by Scots
628 pine shoots: calibration of a stomatal uptake model including the non-stomatal component, *Atmospheric*
629 *Environment*, 38, 2387-2398, doi:10.1016/j.atmosenv.2003.09.077.
630 Atkinson, R., and J. Arey (2003), Gas-phase tropospheric chemistry of biogenic volatile organic compounds: a
631 review, *Atmospheric Environment*, 37, S197-S219, doi:10.1016/s1352-2310(03)00391-1.
632 Bocquet, F., D. Helmig, B. A. Van Dam, and C. W. Fairall (2011), Evaluation of the flux gradient technique for
633 measurement of ozone surface fluxes over snowpack at Summit, Greenland, *Atmospheric Measurement*
634 *Techniques*, 4, 2305-2321, doi:10.5194/amt-4-2305-2011.
635 Bouvier-Brown, N. C., A. H. Goldstein, D. R. Worton, D. M. Matross, J. B. Gilman, W. C. Kuster, D. Welsh-Bon,
636 C. Warneke, J. A. de Gouw, T. M. Cahill, and R. Holzinger (2009a), Methyl chavicol: characterization of its
637 biogenic emission rate, abundance, and oxidation products in the atmosphere, *Atmospheric Chemistry and*
638 *Physics*, 9, 2061-2074.
639 Bouvier-Brown, N. C., R. Holzinger, K. Palitzsch, and A. H. Goldstein (2009b), Large emissions of sesquiterpenes
640 and methyl chavicol quantified from branch enclosure measurements, *Atmospheric Environment*, 43, 389-
641 401, doi:10.1016/j.atmosenv.2008.08.039.
642 Boylan, P., D. Helmig, and J. H. Park (2014), Characterization and mitigation of water vapor effects in the
643 measurement of ozone by chemiluminescence with nitric oxide, *Atmospheric Measurement Techniques*, 7,
644 1231-1244, doi:10.5194/amt-7-1231-2014.
645 Damian, V., Sandu, A., Damian, M., Potra, F., and Carmichael, G. (2002), The kinetic preprocessor KPP—A
646 software environment for solving chemical kinetics, *Computers & Chemical Engineering*, 26, 1567–1579.
647 doi:10.1016/S0098-1354(02)00128-X.
648 Di Carlo, P., W. H. Brune, M. Martinez, H. Harder, R. Leshner, X. R. Ren, T. Thornberry, M. A. Carroll, V. Young, P.
649 B. Shepson, D. Riemer, E. Apel, and C. Campbell (2004), Missing OH reactivity in a forest: Evidence for
650 unknown reactive biogenic VOCs, *Science*, 304, 722-725.
651 Duhl, T. R., D. Helmig, and A. Guenther (2008), Sesquiterpene emissions from vegetation: a review,
652 *Biogeosciences*, 5, 761-777.
653 Fares, S., A. Goldstein, and F. Loreto (2010a), Determinants of ozone fluxes and metrics for ozone risk
654 assessment in plants, *Journal of Experimental Botany*, 61, 629-633, doi:10.1093/jxb/erp336.

655 Fares, S., M. McKay, R. Holzinger, and A. H. Goldstein (2010b), Ozone fluxes in a *Pinus ponderosa* ecosystem
656 are dominated by non-stomatal processes: Evidence from long-term continuous measurements, *Agricultural*
657 *and Forest Meteorology*, 150, 420-431.

658 Fares, S., J. H. Park, E. Ormeno, D. R. Gentner, M. McKay, F. Loreto, J. Karlik, and A. H. Goldstein (2010c), Ozone
659 uptake by citrus trees exposed to a range of ozone concentrations, *Atmospheric Environment*, 44, 3404-3412,
660 doi:10.1016/j.atmosenv.2010.06.010.

661 Goldstein, A. H., M. McKay, M. R. Kurpius, G. W. Schade, A. Lee, R. Holzinger, and R. A. Rasmussen (2004),
662 Forest thinning experiment confirms ozone deposition to forest canopy is dominated by reaction with
663 biogenic VOCs, *Geophysical Research Letters*, 31, doi:L22106
664 10.1029/2004gl021259.

665 Helmig, D., R. Daly, and S. B. Bertman (2010), Ozone reactivity of biogenic volatile organic compounds from
666 four dominant tree species at PROPHET-CABINEX, Abstract A53C-0240, 2010 Fall Meeting, AGU, San
667 Francisco, Calif., 13-17 Dec. .

668 Hogg, A., J. Uddling, D. Ellsworth, M. A. Carroll, S. Pressley, B. Lamb, and C. Vogel (2007), Stomatal and non-
669 stomatal fluxes of ozone to a northern mixed hardwood forest, *Tellus Series B-Chemical and Physical*
670 *Meteorology*, 59, 514-525, doi:10.1111/j.1600-0889.2007.00269.x.

671 Holzinger, R., A. Lee, K. T. Paw, and A. H. Goldstein (2005), Observations of oxidation products above a forest
672 imply biogenic emissions of very reactive compounds, *Atmospheric Chemistry and Physics*, 5, 67-75.

673 Kim, D. J., T. V. Dinh, J. Y. Lee, I. Y. Choi, D. J. Son, I. Y. Kim, Y. Sunwoo, and J. C. Kim (2019), Effects of Water
674 Removal Devices on Ambient Inorganic Air Pollutant Measurements, *International journal of environmental*
675 *research and public health*, 16, 9, doi:10.3390/ijerph16183446.

676 Kim, D. J., T. V. Dinh, J. Y. Lee, D. J. Son, and J. C. Kim (2020), Effect of Nafion Dryer and Cooler on Ambient Air
677 Pollutant (O₃, SO₂, CO) Measurement, *Asian J. Atmos. Environ.*, 14, 28-34, doi:10.5572/ajae.2020.14.1.028.

678 Kim, S., A. Guenther, T. Karl, and J. Greenberg (2011), Branch-level measurement of total OH reactivity for
679 constraining unknown BVOC emission during CABINEX (Community Atmosphere-Biosphere Interactions
680 Experiments)-09 field campaign, *Atmos. Chem. Phys. Discuss.*, 11, 7781-7809.

681 Kurpius, M. R., and A. H. Goldstein (2003), Gas-phase chemistry dominates O₃ loss to a forest, implying a
682 source of aerosols and hydroxyl radicals to the atmosphere, *Geophysical Research Letters*, 30,
683 doi:10.1029/2002gl016785.

684 Lenschow, D. H., R. Pearson, and B. B. Stankov (1981), Estimating the ozone budget in the boundary-layer by
685 use of aircraft measurements of ozone eddy flux and mean concentration, *Journal of Geophysical Research-*
686 *Oceans*, 86, 7291-7297, doi:10.1029/JC086iC08p07291.

687 Lenschow, D. H., R. Pearson, and B. B. Stankov (1982), Measurements of ozone vertical flux to ocean and
688 forest, *Journal of Geophysical Research-Oceans and Atmospheres*, 87, 8833-8837,
689 doi:10.1029/JC087iC11p08833.

690 Lou, S., F. Holland, F. Rohrer, K. Lu, B. Bohn, T. Brauers, C. C. Chang, H. Fuchs, R. Haseler, K. Kita, Y. Kondo, X.
691 Li, M. Shao, L. Zeng, A. Wahner, Y. Zhang, W. Wang, and A. Hofzumahaus (2010), Atmospheric OH reactivities
692 in the Pearl River Delta - China in summer 2006: measurement and model results, *Atmospheric Chemistry*
693 *and Physics*, 10, 11243-11260, doi:10.5194/acp-10-11243-2010.

694 Matsumoto, J. (2014), Measuring Biogenic Volatile Organic Compounds (BVOCs) from Vegetation in Terms of
695 Ozone Reactivity, *Aerosol Air Qual. Res.*, 14, 197-206, doi:10.4209/aaqr.2012.10.0275.

696 Matthews, R. D., R. F. Sawyer, and R. W. Schefer (1977), Interferences in chemiluminescence measurement of
697 NO and NO₂ emissions from combustion systems, *Environ. Sci. Technol.*, 11, 1092-1096.

698 McKinney, K. A., B. H. Lee, A. Vasta, T. V. Pho, and J. W. Munger (2011), Emissions of isoprenoids and
699 oxygenated biogenic volatile organic compounds from a New England mixed forest, *Atmos. Chem. Phys.*, 11,
700 4807-4831.

701 Misztal, P. K., S. M. Owen, A. B. Guenther, R. Rasmussen, C. Geron, P. Harley, G. J. Phillips, A. Ryan, D. P.
702 Edwards, C. N. Hewitt, E. Nemitz, J. Siong, M. R. Heal, and J. N. Cape (2010), Large estragole fluxes from oil
703 palms in Borneo, *Atmospheric Chemistry and Physics*, 10, 4343-4358, doi:10.5194/acp-10-4343-2010.

704 Ortega, J., and D. Helmig (2008), Approaches for quantifying reactive and low-volatility biogenic organic
705 compound emissions by vegetation enclosure techniques - Part A, *Chemosphere*, 72, 343-364,
706 doi:10.1016/j.chemosphere.2007.11.020.

707 Ortega, J., D. Helmig, R. W. Daly, D. M. Tanner, A. B. Guenther, and J. D. Herrick (2008), Approaches for
708 quantifying reactive and low-volatility biogenic organic compound emissions by vegetation enclosure
709 techniques - Part B: Applications, *Chemosphere*, 72, 365-380, doi:10.1016/j.chemosphere.2008.02.054.

710 Ortega, J., D. Helmig, A. Guenther, P. Harley, S. Pressley, and C. Vogel (2007), Flux estimates and OH reaction
711 potential of reactive biogenic volatile organic compounds (BVOCs) from a mixed northern hardwood forest,
712 *Atmospheric Environment*, 41, 5479-5495, doi:10.1016/j.atmosenv.2006.12.033.

713 Park, J., A. B. Guenther, and D. Helmig (2013), Ozone reactivity of biogenic volatile organic compound (BVOC)
714 emissions during the Southeast Oxidant and Aerosol Study (SOAS), in American Geophysical Union, Fall
715 Meeting 2013, abstract #A13A-0172, edited.

716 Ridley, B. A., F. E. Grahek, and J. G. Walega (1992), A small, high-sensitivity, medium-response ozone detector
717 suitable for measurements from light aircraft, *Journal of Atmospheric and Oceanic Technology*, 9, 142-148,
718 doi:10.1175/1520-0426(1992)009<0142:ashsmr>2.0.co;2.

719 Sommariva, R., L. J. Kramer, L. R. Crilley, M. S. Alam, and W. J. Bloss (2020), An instrument for in situ
720 measurement of total ozone reactivity, *Atmospheric Measurement Techniques*, 13, 1655-1670,
721 doi:10.5194/amt-13-1655-2020.

722 Spicer, C. W., D. W. Joseph, and W. M. Ollison (2010), A Re-Examination of Ambient Air Ozone Monitor
723 Interferences, *Journal of the Air & Waste Management Association*, 60, 1353-1364, doi:10.3155/1047-
724 3289.60.11.1353.

725 Wilson, K. L., and J. W. Birks (2006), Mechanism and elimination of a water vapor interference in the
726 measurement of ozone by UV absorbance, *Environmental Science & Technology*, 40, 6361-6367,
727 doi:10.1021/es052590c.

728 Wolfe, G. M., J. A. Thornton, W. A. McKay, and A. H. Goldstein (2011), Forest-atmosphere exchange of ozone:
729 Sensitivity to very reactive biogenic VOC emissions and implications for in-canopy photochemistry, *Atmos.*
730 *Chem. Phys. Discuss.*, 11, 13381-13424.